Available online at www.eccomasproceedia.org
Eccomas Proceedia COMPDYN (2017) 4711-4725

ECCOMAS
Proceedia

COMPDYN 2017
6th ECCOMAS Thematic Conference on
Computational Methods in Structural Dynamics and Earthquake Engineering
M. Papadrakakis, M. Fragiadakis (eds.)
Rhodes Island, Greece, 15–17 June, 2017

THE INFLUENCE OF IMPERFECTLY KNOWN LOCAL SUBSOIL CONDITIONS ON THE PREDICTION OF GROUND-BORNE VIBRATION IN BUILDINGS

Manthos Papadopoulos, Stijn François, Geert Degrande and Geert Lombaert

KU Leuven, Department of Civil Engineering, Structural Mechanics Section
Kasteelpark Arenberg 40, 3001 Leuven, Belgium
e-mail: {manthos.papadopoulos, stijn.francois, geert.degrande, geert.lombaert}@kuleuven.be

Keywords: ground-borne vibrations, dynamic soil-structure interaction, elastic wave propagation, stochastic elastic media, perfectly matched layers; Monte-Carlo simulation.

Abstract. *This paper examines the influence of imperfectly known local subsoil conditions on the response prediction of buildings to ground-borne environmental vibration. A probabilistic finite element-perfectly matched layers model is developed for the analysis of the dynamic soil-structure interaction problem where the shear modulus of the soil is modeled as a conditional random field. An incident wave field is propagated through the finite element-perfectly matched layers model by decomposing the displacement field of the soil in accordance with the subdomain formulation developed for the dynamic soil-structure interaction problem. Monte Carlo simulation is used to propagate the uncertainty on the subsoil properties to the response of a building. A parametric study is performed with respect to the spatial correlation length of the random field representing the shear modulus of the subsoil, and the foundation type of the building. The uncertain subsoil properties affect both the incident wave field exciting the building and the dynamic stiffness of the coupled soil-building system. The uncertainty of the building response varies over frequency bands but as a general trend increases with frequency.*

© 2017 The Authors. Published by Eccomas Proceedia.
Peer-review under responsibility of the organizing committee of COMPDYN 2017.
doi: 10.7712/120117.5756.18370

1 INTRODUCTION

Ground-borne vibration in the built environment are induced by environmental sources like road and railway traffic or construction and industrial activities. The passage of vehicles over uneven roads or tracks and the operation of heavy machinery generate elastodynamic waves that propagate through the soil and impinge on the foundation of nearby structures leading to structural vibrations. These vibrations may lead to malfunctioning of sensitive equipment, discomfort of people and structural damage. Furthermore, noise can be re-radiated from floors and walls.

Dynamic soil-structure interaction plays a crucial role in the prediction of the response of structures due to ground-borne vibration. Studies on dynamic soil-structure interaction initiated in the field of earthquake engineering for the design and construction of structures of high importance [1]. More recently, the growing traffic volume, the development of high-speed railway lines and the expansion of underground transportation networks in densely populated urban areas have lead to an interest in the problem for environmental vibration where building on the prior developments computational models have been developed for both the prediction of the induced incident wave field and the structural response [2].

In these models, the soil is commonly idealized as a horizontally stratified visco-elastic half-space composed by homogeneous layers. However, geotechnical investigations suggest that the soil properties exhibit considerable spatial variability even within apparently homogeneous soil deposits [3]. This variability is mainly attributed to the physical processes involved in the formation of the soil layers but also to man-made activities that may perturb the properties of virgin land. Since the soil directly beneath a building can have a predominant role in its response [4], the aim of this paper is to assess the influence of imperfectly known local subsoil conditions on the response predictions of buildings to ground-borne induced vibrations.

The paper starts with introduction of the dynamic soil-structure interaction model and the particularities of incorporating an incident wave field in the analysis. Next, the modeling of the stochastic subsoil is discussed. Finally, the results of a parametric study involving investigation with respect to the spatial correlation length of the random field representing the shear modulus of the subsoil, and the foundation type of the building are presented.

2 METHOD OF ANALYSIS

In dynamic soil-structure interaction computational models, the semi-infinite extent of the soil needs to be taken into account by allowing the radiation of elastodynamic waves to infinity. This is achieved by using either coupled finite element (FE)-boundary element (BE) formulations [5] or finite element formulations in conjunction with absorbing boundary conditions (ABC) [6, 7] or perfectly matched layers (PML) [8]. Both the coupled FE-BE formulations and the FE formulations with ABC or PML have advantages and disadvantages that make them preferable for different problem settings. For the applications of this paper, a FE-PML formulation is used as it proved computationally more efficient.

2.1 The dynamic soil-structure interaction model

Figure 1a depicts the dynamic soil-structure interaction problem considered in this work. The building Ω_{b} is surrounded by a bounded volume of subsoil $\Omega_{\mathrm{s}}^{\mathrm{i}}$ with imperfectly known properties whereas the rest of the subsoil $\Omega_{\mathrm{s}}^{\mathrm{e}}$ is considered well known. The building is excited by an incident wave field $\hat{\mathbf{u}}_{\mathrm{inc}}$, where the hat above the variable denotes its representation in the frequency domain. Figure 1b shows how this problem is modeled by means of finite elements

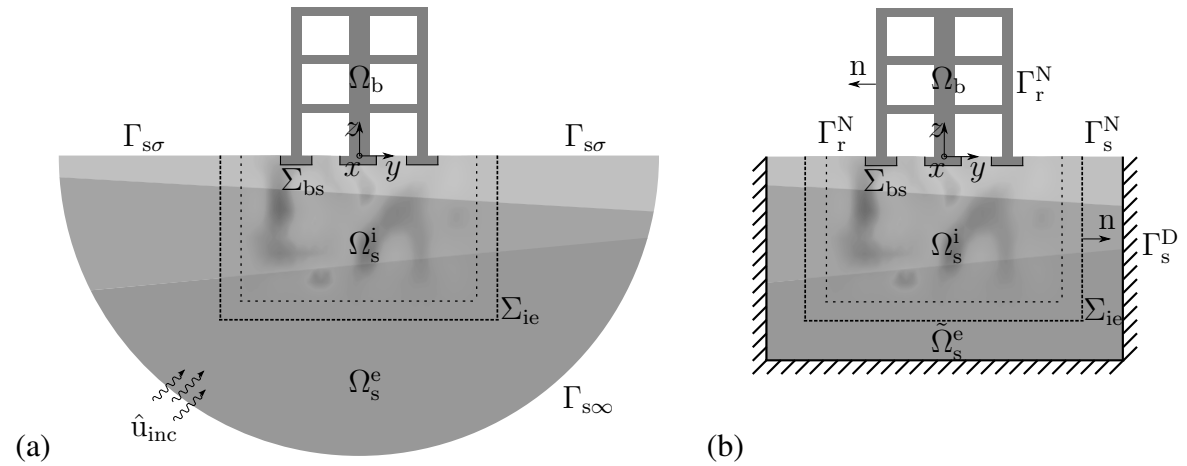

Figure 1: (a) Dynamic soil-structure interaction problem and (b) FE-PML model.

and perfectly matched layers. The computational domain Ω is divided into the regular domain $\Omega_{\mathrm{r}} = \Omega_{\mathrm{b}} \cup \Omega_{\mathrm{s}}^{\mathrm{i}}$ and the PML buffer zone $\tilde{\Omega}_{\mathrm{s}}^{\mathrm{e}}$ surrounding this domain. The regular domain Ω_{r} is modeled with FE where the material properties of $\Omega_{\mathrm{s}}^{\mathrm{i}}$ are modeled as conditional random fields (section 2.3) with a small zone close to the boundaries of this domain having deterministic properties. The PML buffer zone $\tilde{\Omega}_{\mathrm{s}}^{\mathrm{e}}$ aims to simulate the truncated unbounded soil $\Omega_{\mathrm{s}}^{\mathrm{e}}$ at the limits of the regular domain Σ_{ie}. The soil-foundation interface is denoted as Σ_{bs}. The FE-PML model is developed based on the three-dimensional elastodynamic equations in the frequency domain.

In order to artificially attenuate the elastodynamic waves that enter into the PML buffer zone, complex coordinate stretching is applied in $\tilde{\Omega}_{\mathrm{s}}^{\mathrm{e}}$. For a coordinate s, representing the x, y or z coordinate, the stretched coordinate $\tilde{s}$ is defined as [8]:

$$\tilde{s} = \int_0^s \hat{\lambda}_{\mathrm{s}}(s)\,\mathrm{d}s = s_{\mathrm{o}} + \int_{s_{\mathrm{o}}}^{s_{\mathrm{t}}} \hat{\lambda}_{\mathrm{s}}(s)\,\mathrm{d}s \tag{1}$$

The stretch function $\hat{\lambda}_{\mathrm{s}}$ is defined as:

$$\hat{\lambda}_{\mathrm{s}}(s) = \alpha_{0\mathrm{s}}(s) + \frac{\alpha_{1\mathrm{s}}(s)}{i\omega} \tag{2}$$

where $\alpha_{0\mathrm{s}}$ and $\alpha_{1\mathrm{s}}$ are polynomial functions that control the amplitude attenuation of the evanescent and propagating waves inside the PML buffer zone, and $\omega \in R$ is the frequency of analysis. The FE system of equations is written in the frequency domain as:

$$\hat{\mathbf{K}}\underline{\hat{\mathbf{u}}} = \underline{\hat{\mathbf{f}}} \tag{3}$$

where $\hat{\mathbf{K}} = \mathbf{K} + (i\omega)^2\,\mathbf{M}$ is the dynamic stiffness matrix of the system with $\mathbf{K} \in \mathrm{C}^{\mathrm{n}\times\mathrm{n}}$ and $\mathbf{M} \in \mathrm{C}^{\mathrm{n}\times\mathrm{n}}$ the stiffness and mass matrix with n the number of degrees of freedom in the model. The vector $\underline{\hat{\mathbf{u}}} \in \mathrm{C}^{\mathrm{n}\times 1}$ collects the nodal displacements while $\underline{\hat{\mathbf{f}}} \in \mathrm{C}^{\mathrm{n}\times 1}$ collects the equivalent nodal loads. Equation (3) can be rewritten in an expanded form according to the subdomain definitions of figure 1:

$$\begin{bmatrix} \hat{\mathbf{K}}_{\mathrm{bb}} & \hat{\mathbf{K}}_{\mathrm{b}\Sigma_{\mathrm{bs}}} & \mathbf{0} \\ \hat{\mathbf{K}}_{\Sigma_{\mathrm{bs}}\mathrm{b}} & \hat{\mathbf{K}}_{\Sigma_{\mathrm{bs}}\Sigma_{\mathrm{bs}}}(\theta) & \hat{\mathbf{K}}_{\Sigma_{\mathrm{bs}}\mathrm{s}}(\theta) \\ \mathbf{0} & \hat{\mathbf{K}}_{\mathrm{s}\Sigma_{\mathrm{bs}}}(\theta) & \hat{\mathbf{K}}_{\mathrm{ss}}(\theta) \end{bmatrix} \begin{Bmatrix} \underline{\hat{\mathbf{u}}}_{\mathrm{b}} \\ \underline{\hat{\mathbf{u}}}_{\Sigma_{\mathrm{bs}}} \\ \underline{\hat{\mathbf{u}}}_{\mathrm{s}} \end{Bmatrix} = \begin{Bmatrix} \underline{\hat{\mathbf{f}}}_{\mathrm{b}} \\ \underline{\hat{\mathbf{f}}}_{\Sigma_{\mathrm{bs}}} \\ \underline{\hat{\mathbf{f}}}_{\mathrm{s}} \end{Bmatrix} \tag{4}$$

where θ denotes an elementary event of the event space Θ. Since the material properties in $\Omega_{\mathrm{s}}^{\mathrm{i}}$ are modeled as random fields, the corresponding dynamic stiffness block matrices in equation (4) are also stochastic. The mapping of the stochastic material properties of $\Omega_{\mathrm{s}}^{\mathrm{i}}$ onto the finite element model is briefly discussed in section 2.3.

To facilitate the subsequent discussion, it is useful to rewrite equation (4) by dynamically condensing the degrees of freedom of the soil $\underline{\hat{\mathbf{u}}}_{\mathrm{s}}$ on the degrees of freedom $\underline{\hat{\mathbf{u}}}_{\Sigma_{\mathrm{bs}}}$ of the soil-foundation interface Σ_{bs}:

$$\begin{bmatrix} \hat{\mathbf{K}}_{\mathrm{bb}} & \hat{\mathbf{K}}_{\mathrm{b}\Sigma_{\mathrm{bs}}} \\ \hat{\mathbf{K}}_{\Sigma_{\mathrm{bs}}\mathrm{b}} & \hat{\tilde{\mathbf{K}}}_{\Sigma_{\mathrm{bs}}\Sigma_{\mathrm{bs}}}(\theta) \end{bmatrix} \begin{Bmatrix} \underline{\hat{\mathbf{u}}}_{\mathrm{b}} \\ \underline{\hat{\mathbf{u}}}_{\Sigma_{\mathrm{bs}}} \end{Bmatrix} = \begin{Bmatrix} \underline{\hat{\mathbf{f}}}_{\mathrm{b}} \\ \underline{\hat{\tilde{\mathbf{f}}}}_{\Sigma_{\mathrm{bs}}}(\theta) \end{Bmatrix} \tag{5}$$

with $\underline{\hat{\tilde{\mathbf{f}}}}_{\Sigma_{\mathrm{bs}}} = \underline{\hat{\mathbf{f}}}_{\Sigma_{\mathrm{bs}}} - \hat{\mathbf{K}}_{\Sigma_{\mathrm{bs}}\mathrm{s}}\hat{\mathbf{K}}_{\mathrm{ss}}^{-1}\underline{\hat{\mathbf{f}}}_{\mathrm{s}}$ and $\hat{\tilde{\mathbf{K}}}_{\Sigma_{\mathrm{bs}}\Sigma_{\mathrm{bs}}}$ the Schur complement of $\hat{\mathbf{K}}_{\mathrm{ss}}$ on $\hat{\mathbf{K}}_{\Sigma_{\mathrm{bs}}\Sigma_{\mathrm{bs}}}$:

$$\hat{\tilde{\mathbf{K}}}_{\Sigma_{\mathrm{bs}}\Sigma_{\mathrm{bs}}} = \hat{\mathbf{K}}_{\Sigma_{\mathrm{bs}}\Sigma_{\mathrm{bs}}} - \hat{\mathbf{K}}_{\Sigma_{\mathrm{bs}}\mathrm{s}}\hat{\mathbf{K}}_{\mathrm{ss}}^{-1}\hat{\mathbf{K}}_{\mathrm{s}\Sigma_{\mathrm{bs}}} \tag{6}$$

2.2 Incorporation of an incident wave field

In order to propagate an incident wave field $\hat{\mathbf{u}}_{\mathrm{inc}}$ generated by a remote excitation source in $\Omega_{\mathrm{s}}^{\mathrm{e}}$ through the FE-PML model, an equivalent traction field $\hat{\mathbf{t}}^{\mathbf{n}}$ on the interface Σ_{ie} needs first to be determined. This traction field is defined based on a methodology where the displacement field of the soil in $\Omega_{\mathrm{s}}^{\mathrm{e}}$ is decomposed in accordance with the subdomain formulation of the soil-structure interaction problem as was originally conceived for FE-BE formulations [9]. The displacement field $\hat{\mathbf{u}}_{\mathrm{s}}^{\mathrm{e}}$ in the exterior soil $\Omega_{\mathrm{s}}^{\mathrm{e}}$ is decomposed as (figure 2):

$$\hat{\mathbf{u}}_{\mathrm{s}}^{\mathrm{e}} = \hat{\mathbf{u}}_{\mathrm{inc}} + \hat{\mathbf{u}}_{\mathrm{d0}} + \hat{\mathbf{u}}_{\mathrm{sc}} \tag{7}$$

In this expression, $\hat{\mathbf{u}}_{\mathrm{inc}}$ is the displacement field of the globally deterministic soil $\Omega_{\mathrm{s}} = \Omega_{\mathrm{s}}^{\mathrm{e}} \cup \Omega_{\mathrm{s}}^{\mathrm{i,det}}$ due to a remote excitation source (figure 2b), $\hat{\mathbf{u}}_{\mathrm{d0}}$ is the locally diffracted displacement field radiated in the exterior soil $\Omega_{\mathrm{s}}^{\mathrm{e}}$ with excavated the interior soil $\Omega_{\mathrm{s}}^{\mathrm{i}}$ for which applies $\hat{\mathbf{u}}_{\mathrm{d0}|\Sigma_{\mathrm{ie}}} = -\hat{\mathbf{u}}_{\mathrm{inc}|\Sigma_{\mathrm{ie}}}$ on the interface Σ_{ie} (figure 2c), and $\hat{\mathbf{u}}_{\mathrm{sc}}$ is the stochastic diffracted displacement field radiated in the exterior soil $\Omega_{\mathrm{s}}^{\mathrm{e}}$ due to the displacements of the stochastic interior soil $\Omega_{\mathrm{s}}^{\mathrm{i}}$ on the interface Σ_{ie} (figure 2d).

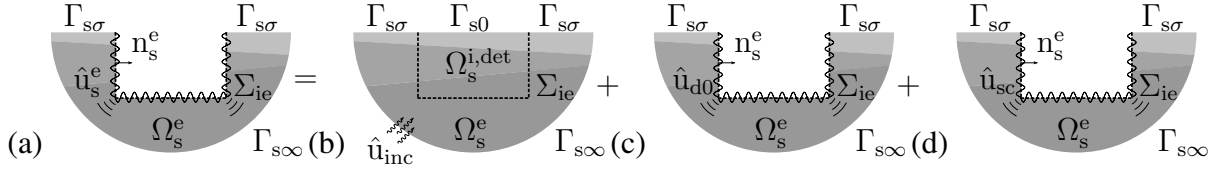

Figure 2: Decomposition of (a) the displacement field $\hat{\mathbf{u}}_{\mathrm{s}}^{\mathrm{e}}$ of the exterior soil $\Omega_{\mathrm{s}}^{\mathrm{e}}$ into (b) the incident wave field $\hat{\mathbf{u}}_{\mathrm{inc}}$ of the globally deterministic soil $\Omega_{\mathrm{s}} = \Omega_{\mathrm{s}}^{\mathrm{e}} \cup \Omega_{\mathrm{s}}^{\mathrm{i,det}}$, (c) the locally diffracted displacement field $\hat{\mathbf{u}}_{\mathrm{d0}}$ and (d) the diffracted displacement field $\hat{\mathbf{u}}_{\mathrm{sc}}$.

On the interface Σ_{ie}, the compatibility condition $\hat{\mathbf{u}}_{\mathrm{s}}^{\mathrm{i}} = \hat{\mathbf{u}}_{\mathrm{s}}^{\mathrm{e}}$ applies and the equilibrium equation reads as:

$$\hat{\mathbf{t}}^{\mathbf{n}}\left(\hat{\mathbf{u}}_{\mathrm{s}}^{\mathrm{i}}\right) + \hat{\mathbf{t}}^{\mathbf{n_s^e}}\left(\hat{\mathbf{u}}_{\mathrm{s}}^{\mathrm{e}}\right) = \mathbf{0} \quad \text{on } \Sigma_{\mathrm{ie}} \tag{8}$$

where $\hat{\mathbf{t}}^{\mathbf{n}}\left(\hat{\mathbf{u}}_{\mathrm{s}}^{\mathrm{i}}\right)$ and $\hat{\mathbf{t}}^{\mathbf{n_s^e}}\left(\hat{\mathbf{u}}_{\mathrm{s}}^{\mathrm{e}}\right)$ are the traction fields imposed on the interface Σ_{ie} by the stochastic interior soil $\Omega_{\mathrm{s}}^{\mathrm{i}}$ and the deterministic exterior soil $\Omega_{\mathrm{s}}^{\mathrm{e}}$, respectively. Subsequently, the decomposition of equation (7) is introduced in equation (8):

$$\hat{\mathbf{t}}^{\mathbf{n}}\left(\hat{\mathbf{u}}_{\mathrm{s}}^{\mathrm{i}}\right)+\hat{\mathbf{t}}^{\mathbf{n_s^e}}\left(\hat{\mathbf{u}}_{\mathrm{sc}}\right)=\underbrace{-\hat{\mathbf{t}}^{\mathbf{n_s^e}}\left(\hat{\mathbf{u}}_{\mathrm{inc}}\right)-\hat{\mathbf{t}}^{\mathbf{n_s^e}}\left(\hat{\mathbf{u}}_{\mathrm{d0}}\right)}_{\hat{\hat{\mathbf{t}}}^{\mathrm{n}}}\quad\text{on }\Sigma_{\mathrm{ie}} \tag{9}$$

The resultant tractions on the left hand side of equation (9) are the stochastic tractions imposed on the interface Σ_{ie} by $\Omega_{\mathrm{s}}=\Omega_{\mathrm{s}}^{\mathrm{e}}\cup\Omega_{\mathrm{s}}^{\mathrm{i}}$, whereas the resultant tractions on the right hand side of the equation are the required deterministic tractions $\hat{\hat{\mathbf{t}}}^{\mathrm{n}}$ on the interface Σ_{ie} to propagate the exterior incident wave field $\hat{\mathbf{u}}_{\mathrm{inc}}$ through the stochastic interior soil $\Omega_{\mathrm{s}}^{\mathrm{i}}$.

The weak form of equation (9) is obtained by considering a virtual displacement field $\hat{\mathbf{v}}$ over the interface Σ_{ie} where after using the same shape functions as for the FE-PML model discretization, the following set of equations is obtained:

$$\int_{\Sigma_{\mathrm{ie}}}\mathbf{N}^{\mathrm{T}}\hat{\mathbf{t}}^{\mathbf{n}}\left(\hat{\mathbf{u}}_{\mathrm{s}}^{\mathrm{i}}\right)\mathrm{d}\Gamma+\int_{\Sigma_{\mathrm{ie}}}\mathbf{N}^{\mathrm{T}}\hat{\mathbf{t}}^{\mathbf{n_s^e}}\left(\hat{\mathbf{u}}_{\mathrm{sc}}\right)\mathrm{d}\Gamma= \underbrace{-\int_{\Sigma_{\mathrm{ie}}}\mathbf{N}^{\mathrm{T}}\hat{\mathbf{t}}^{\mathbf{n_s^e}}\left(\hat{\mathbf{u}}_{\mathrm{inc}}\right)\mathrm{d}\Gamma-\int_{\Sigma_{\mathrm{ie}}}\mathbf{N}^{\mathrm{T}}\hat{\mathbf{t}}^{\mathbf{n_s^e}}\left(\hat{\mathbf{u}}_{\mathrm{d0}}\right)\mathrm{d}\Gamma}_{\left\{\mathbf{0},\,\mathbf{0},\,\underline{\hat{\mathbf{f}}}_{\mathrm{s}}\right\}^{\mathrm{T}}} \tag{10}$$

The left hand side of equation (10) corresponds now to the dynamic impedance of the FE-PML model on interface Σ_{ie}, while the right hand side contains the required equivalent nodal forces on the interface Σ_{ie} that represent the exterior incident wave field $\hat{\mathbf{u}}_{\mathrm{inc}}$.

The deterministic displacement field $\hat{\mathbf{u}}_{\mathrm{inc}}$ and traction field $\hat{\mathbf{t}}_{\mathrm{inc}}=\hat{\mathbf{t}}^{\mathbf{n_s^e}}\left(\hat{\mathbf{u}}_{\mathrm{inc}}\right)$ of the globally deterministic soil $\Omega_{\mathrm{s}}=\Omega_{\mathrm{s}}^{\mathrm{e}}\cup\Omega_{\mathrm{s}}^{\mathrm{i,det}}$ are computed using a source model, generally assuming that the coupling between the subproblems of the source and the receiver can be disregarded [10]. In the present work, the direct stiffness method is used for this purpose [11].

The second integral on the right-hand side of equation (10) is not computed directly as the traction field $\hat{\mathbf{t}}_{\mathrm{d0}}=\hat{\mathbf{t}}^{\mathbf{n_s^e}}\left(\hat{\mathbf{u}}_{\mathrm{d0}}\right)$ is not known a priori. Instead, the integral is implicitly evaluated through the displacement field $\hat{\mathbf{u}}_{\mathrm{inc}}$ on the interface Σ_{ie}. According to the definition of the locally diffracted displacement field $\hat{\mathbf{u}}_{\mathrm{d0}}$, this problem boils down to computing the reaction forces $\underline{\hat{\mathbf{r}}}_{\Sigma_{\mathrm{ie}}}^{\mathrm{e}}=\underline{\hat{\mathbf{r}}}_{\Sigma_{\mathrm{ie}}}^{\mathrm{e}}\left(\hat{\mathbf{u}}_{\mathrm{d0}|\Sigma_{\mathrm{ie}}}\right)$ on the interface Σ_{ie} of the FE-PML model with excavated the interior soil $\Omega_{\mathrm{s}}^{\mathrm{i}}$ due to imposed displacements $\hat{\mathbf{u}}_{\mathrm{d0}|\Sigma_{\mathrm{ie}}}=-\hat{\mathbf{u}}_{\mathrm{inc}|\Sigma_{\mathrm{ie}}}$ on the interface Σ_{ie} (figure 3). The FE-PML system of equations of the truncated exterior soil $\tilde{\Omega}_{\mathrm{s}}^{\mathrm{e}}$ due to imposed displacements $\underline{\hat{\mathbf{u}}}_{\Sigma_{\mathrm{ie}}}^{\mathrm{e}}$ on the interface Σ_{ie} is:

$$\begin{bmatrix}\hat{\mathbf{K}}_{\Sigma_{\mathrm{ie}}\Sigma_{\mathrm{ie}}}^{\mathrm{e}} & \hat{\mathbf{K}}_{\Sigma_{\mathrm{ie}}\mathrm{s}}^{\mathrm{e}}\\ \hat{\mathbf{K}}_{\mathrm{s}\Sigma_{\mathrm{ie}}}^{\mathrm{e}} & \hat{\mathbf{K}}_{\mathrm{ss}}^{\mathrm{e}}\end{bmatrix}\begin{Bmatrix}\underline{\hat{\mathbf{u}}}_{\Sigma_{\mathrm{ie}}}^{\mathrm{e}}\\ \underline{\hat{\mathbf{u}}}_{\mathrm{s}}^{\mathrm{e}}\end{Bmatrix}=\begin{Bmatrix}\underline{\hat{\mathbf{r}}}_{\Sigma_{\mathrm{ie}}}^{\mathrm{e}}\\ \mathbf{0}\end{Bmatrix} \tag{11}$$

with $\underline{\hat{\mathbf{u}}}_{\Sigma_{\mathrm{ie}}}^{\mathrm{e}}=\hat{\mathbf{u}}_{\mathrm{d0}|\Sigma_{\mathrm{ie}}}=-\hat{\mathbf{u}}_{\mathrm{inc}|\Sigma_{\mathrm{ie}}}$. Rearranging and solving this system with respect to $\underline{\hat{\mathbf{r}}}_{\Sigma_{\mathrm{ie}}}^{\mathrm{e}}$ yields:

$$\underline{\hat{\mathbf{r}}}_{\Sigma_{\mathrm{ie}}}^{\mathrm{e}}\left(-\hat{\mathbf{u}}_{\mathrm{inc}|\Sigma_{\mathrm{ie}}}\right)=\left(\hat{\mathbf{K}}_{\mathrm{s}\Sigma_{\mathrm{ie}}}^{\mathrm{e}}\hat{\mathbf{K}}_{\mathrm{ss}}^{\mathrm{e}-1}\hat{\mathbf{K}}_{\mathrm{s}\Sigma_{\mathrm{ie}}}^{\mathrm{e}}-\hat{\mathbf{K}}_{\Sigma_{\mathrm{ie}}\Sigma_{\mathrm{ie}}}^{\mathrm{e}}\right)\hat{\mathbf{u}}_{\mathrm{inc}|\Sigma_{\mathrm{ie}}} \tag{12}$$

The required nodal loads $\underline{\hat{\mathbf{f}}}_{\mathrm{s}}$ due to an incident wave field are finally obtained as:

$$\begin{Bmatrix}\mathbf{0}\\ \mathbf{0}\\ \underline{\hat{\mathbf{f}}}_{\mathrm{s}}\end{Bmatrix}\simeq-\int_{\Sigma_{\mathrm{ie}}}\mathbf{N}^{\mathrm{T}}\hat{\mathbf{t}}^{\mathbf{n_s^e}}\left(\hat{\mathbf{u}}_{\mathrm{inc}}\right)\mathrm{d}\Gamma-\begin{Bmatrix}\mathbf{0}\\ \mathbf{0}\\ \underline{\hat{\mathbf{r}}}^{\mathrm{e}}\end{Bmatrix} \tag{13}$$

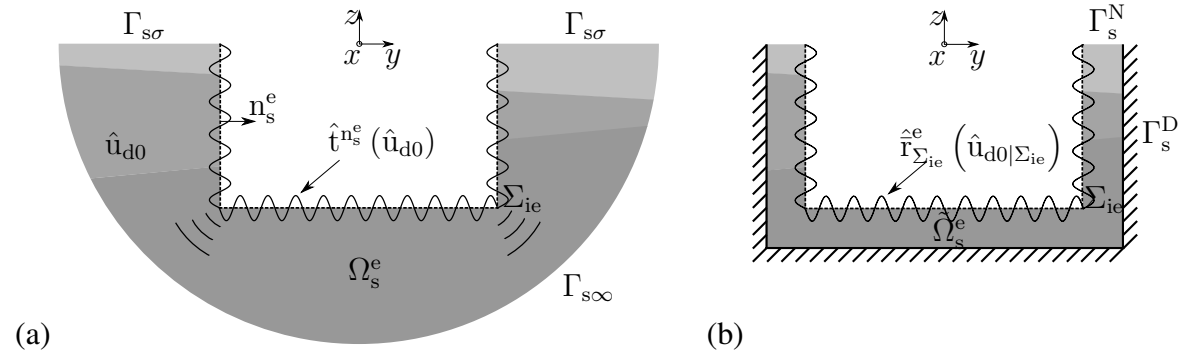

Figure 3: (a) Locally diffracted displacement field $\hat{\mathbf{u}}_{\mathrm{d0}}$ and (b) FE-PML model of the truncated exterior soil $\tilde{\Omega}_{\mathrm{s}}^{\mathrm{e}}$.

where $\hat{\underline{\mathbf{r}}}^{\mathrm{e}} = \left\{\hat{\underline{\mathbf{r}}}^{\mathrm{e}}_{\Sigma_{\mathrm{ie}}},\, \mathbf{0}\right\}^{\mathrm{T}}$ according to equation (11).

2.3 Stochastic subsoil modeling

The subsoil in $\Omega_{\mathrm{s}}^{\mathrm{i}}$ is modeled as a heterogeneous isotropic elastic medium with imperfectly known material properties. In the present paper, the characterization of the elastic properties of the subsoil is based on its shear modulus G and Poisson's ratio ν. The shear modulus is selected as an elastic parameter to characterize the subsoil because some of its statistical properties can be implicitly elicited from cone penetration test (CPT) data for which a large database is available [12]. Because the variation of the Poisson's ratio ν and the material density ρ within soil deposits is rather small, their values are fairly considered as deterministic. Hence, the investigation focuses only on the shear modulus G of the subsoil in the following.

The shear modulus G of the subsoil in $\Omega_{\mathrm{s}}^{\mathrm{i}}$ is modeled as a random field $G(\boldsymbol{x}, \theta)$ defined over the parameter space $\boldsymbol{x} \in \Omega_{\mathrm{s}}^{\mathrm{i}}$ [13]. Since the complete probabilistic characterization of the shear modulus $G(\boldsymbol{x}, \theta)$ is infeasible, its description relies only on its second order statistics. Thus, the information on the shear modulus $G(\boldsymbol{x}, \theta)$ limited to its marginal probability distribution function (PDF) $p_{\mathrm{G}}(\theta)$, mean $\mu_{\mathrm{G}}(\boldsymbol{x})$, variance $\sigma_{\mathrm{G}}^2(\boldsymbol{x})$ and auto-correlation coefficient $\rho_{\mathrm{GG}}(\boldsymbol{x}, \boldsymbol{x'})$. Because the shear modulus $G(\boldsymbol{x}, \theta)$ should take strictly positive values, the Gamma distribution is opted as its marginal PDF. The covariance function $C_{\mathrm{GG}}(\boldsymbol{x}, \boldsymbol{x'})$ is defined as:

$$C_{\mathrm{GG}}(\boldsymbol{x}, \boldsymbol{x'}) = \sigma_{\mathrm{G}}(\boldsymbol{x})\, \sigma_{\mathrm{G}}(\boldsymbol{x'})\, \rho_{\mathrm{GG}}(\boldsymbol{x}, \boldsymbol{x'}) \tag{14}$$

The stochastic shear modulus $G(\boldsymbol{x}, \theta)$ is simulated through a translation process based on the Nataf multivariate distribution [14]. The non-Gaussian shear modulus $G(\boldsymbol{x}, \theta)$ is defined as a non-linear function of an underlying Gaussian random field $\mathcal{G}(\boldsymbol{x}, \theta)$ as:

$$G(\boldsymbol{x}, \theta) = P_{\Gamma}^{-1}\left(P_{\mathrm{N}}\left(\frac{\mathcal{G}(\boldsymbol{x}, \theta) - \mu_{\mathcal{G}}(\boldsymbol{x})}{\sigma_{\mathcal{G}}(\boldsymbol{x})}\right)\right) \tag{15}$$

where P_{Γ}^{-1} is the inverse of the target Gamma marginal cumulative distribution (CDF), P_{N} is the standard normal CDF function, and $\mu_{\mathcal{G}}(\boldsymbol{x}) = \mu_{\mathrm{G}}(\boldsymbol{x})$ and $\sigma_{\mathcal{G}}(\boldsymbol{x}) = \sigma_{\mathrm{G}}(\boldsymbol{x})$ are respectively the mean and variance of $\mathcal{G}(\boldsymbol{x}, \theta)$. Furthermore, because matching material properties at the interface between $\Omega_{\mathrm{s}}^{\mathrm{i}}$ and $\Omega_{\mathrm{s}}^{\mathrm{e}}$ are desirable, the shear modulus $G(\boldsymbol{x}, \theta)$ is modeled as a conditional random field $\bar{G}(\boldsymbol{x}, \theta)$ with prescribed deterministic values at the interface Σ_{ie} [13].

In order to generate realizations of the shear modulus $\bar{G}(\boldsymbol{x}, \theta)$, it is necessary to reduce its infinite dimensionality into a finite set of random variables. In this work, this is achieved by

discretizing the continuous parameter space $\boldsymbol{x} \in \Omega_{\mathrm{s}}^{\mathrm{i}}$ into a finite set of control points $\boldsymbol{x}_k \in \Omega_{\mathrm{s}}^{\mathrm{i}}$ with $k \in \{1, ..., n_{\mathrm{k}}\}$ [15]. After discretization, the random field $\bar{G}(\boldsymbol{x}, \theta)$ is represented by a random vector $\bar{\mathbf{G}}(\theta)$ corresponding to the evaluation of the random field at the set of control points $\boldsymbol{x}_k$. Realizations of the random vector $\bar{\boldsymbol{\mathcal{G}}}(\theta)$ can be then generated as:

$$\bar{\boldsymbol{\mathcal{G}}}(\theta) \approx \boldsymbol{\mu}_{\boldsymbol{\mathcal{G}}} + \sum_{k=1}^{n_{\mathrm{m}}} \xi_k(\theta) \sqrt{\lambda_k} \boldsymbol{\phi}_k \tag{16}$$

where λ_k and $\boldsymbol{\phi}_k$ are the k-th eigenvalue and eigenvector of the covariance matrix $\bar{\mathbf{C}}_{\boldsymbol{\mathcal{G}}\boldsymbol{\mathcal{G}}}$ respectively, and $\xi_k(\theta)$ are random variables sampled from the standard Gaussian distribution $\mathcal{N}(0, 1)$. In order to improve the representativeness of the sampled pool of realizations, Latin hypercube sampling with artificial correlation reduction is used in the present paper [16]. This sampling scheme explores the event space more uniformly avoiding the formation of clusters of realizations that might stall convergence in a Monte Carlo simulation. The number $n_{\mathrm{m}} \leq n_{\mathrm{k}}$ of eigenpairs (λ_k, $\boldsymbol{\phi}_k$) included in the expansion of equation (16) can be decided based on a maximum acceptable relative truncation error:

$$\epsilon(n_{\mathrm{m}}) = 1 - \frac{1}{\mathrm{Tr}\left(\bar{\mathbf{C}}_{\boldsymbol{\mathcal{G}}\boldsymbol{\mathcal{G}}}\right)} \sum_{k=1}^{n_{\mathrm{m}}} \lambda_k \leq \epsilon_{\max} \tag{17}$$

where $\mathrm{Tr}(\cdot)$ denotes the trace of a matrix.

In equation (4), the dynamic stiffness block matrices are formulated by taking into account the continuous variation of the shear modulus $\bar{G}(\boldsymbol{x}, \theta)$ in $\Omega_{\mathrm{s}}^{\mathrm{i}}$. The stochastic shear modulus $\bar{\mathbf{G}}(\theta)$ is first evaluated at the finite element nodes and subsequently interpolated at any point of domain $\Omega_{\mathrm{s}}^{\mathrm{i}}$ by using the same FE shape functions as for the interpolation of the displacements [17].

3 PARAMETRIC STUDY

The influence of the imperfectly known local subsoil conditions on the response predictions of buildings to ground-borne vibration is assessed in a parametric study. To this end, a three story reinforced concrete office building is considered with the dimensions shown in table 1. The Young's modulus of the building is $E_{\mathrm{s}} = 30\,\mathrm{GPa}$ while its material density is $\rho_{\mathrm{s}} = 2500\,\mathrm{kg/m^3}$. Figure 4 shows the i-th floor layout of the building. Two different cases are

h_{s} [m]	t_{s} [m]	C [m × m]	B [m × m]	W_x [m × m]	W_y [m × m]
3	0.15	0.35 × 0.35	0.20 × 0.50	1.50 × 0.20	0.20 × 1.50

Table 1: R/C building characteristics.

examined for the building's foundation: a) a uniform raft foundation with thickness $t_{\mathrm{f}} = 0.60$ m, and b) individual footings for each column and wall with a thickness of $t_{\mathrm{f}} = 0.40$ m. The soil underneath the building is modeled as a visco-elastic half-space with the mean properties shown in table 2. The building response is investigated by computing transfer functions which relate its displacements to a point load applied at the surface of the soil at the point $\boldsymbol{S}(-34\,\mathrm{m}, -26\,\mathrm{m}, 0\,\mathrm{m})$ with respect to the origin of the reference system. The analysis is performed in the frequency range between 1 Hz and 80 Hz which is of interest for problems of environmental ground vibration.

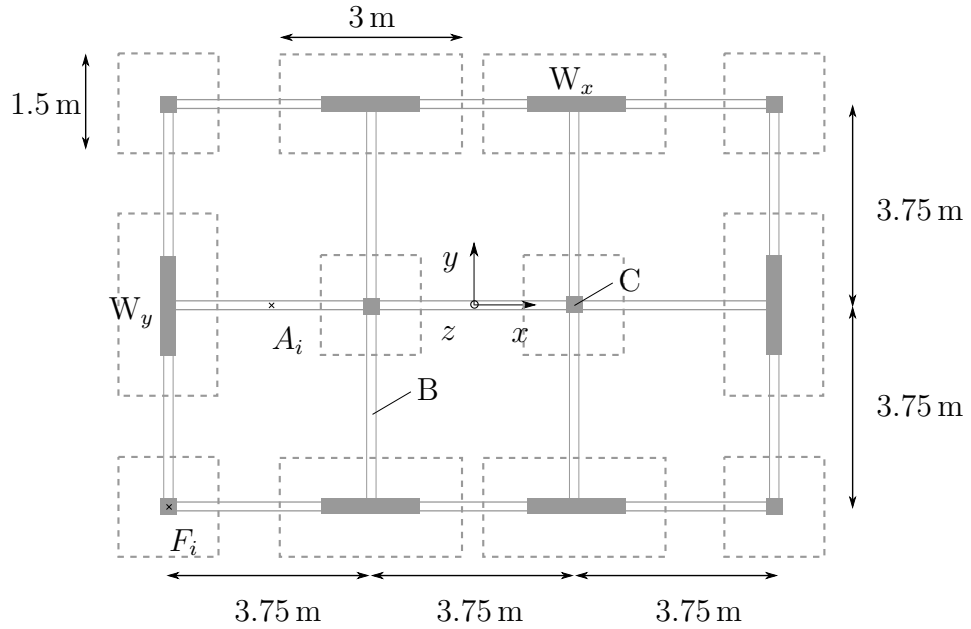

Figure 4: Building layout at the i-th floor where W_x and W_y stands for the walls in the x and the y direction, C stands for the columns and B for the beams. The outline of the foundation footings is also shown with dashed lines. The receiver locations A_i and F_i at the i-th floor are indicated with $\times$.

h [m]	C_s [m/s]	C_p [m/s]	G [MPa]	ν [$-$]	ρ [kg/m^3]	β [$-$]
∞	300	600	162	1/3	1800	0.01

Table 2: Subsoil mean properties.

Figure 5 shows the FE-PML model. The subsoil is discretized with three-dimensional twenty-node finite elements. A maximum element size $l_\mathrm{e} = 0.75$ m is used for the mesh, corresponding to 5 quadratic finite elements per shear wavelength λ_s at a frequency of 80 Hz. The building is modeled with frame and eight-node shell elements. Hysteretic damping is assumed for the building with $\eta = 2\xi = 0.05$.

The shear modulus of the soil in $\Omega_\mathrm{s}^\mathrm{i}$ (figure 5) is modeled as a conditional random field $\bar{G}\left(\boldsymbol{x}, \theta\right)$ with a Gamma marginal PDF and a coefficient of variation $\mathrm{CoV} = 0.25$ according to the methodology outlined in section 2.3. An isotropic squared exponential correlation coefficient function is assumed for the covariance of the unconditional random field $G\left(\boldsymbol{x}, \theta\right)$ which ensures continuous field realizations:

$$C_\mathrm{GG}(\boldsymbol{x}, \boldsymbol{x'}) = \sigma_\mathrm{G}^2 \exp\left(-\frac{|\boldsymbol{x} - \boldsymbol{x'}|^2}{l_\mathrm{c}^2}\right) \tag{18}$$

In general, the variation of the material properties in soil deposits is anisotropic as the correlation length in the vertical and horizontal directions are not the same. However, in order to develop a general understanding of how the spatial variability of the subsoil properties influences the response predictions of buildings, a single isotropic correlation length is considered in the present paper. The correlation length l_c of the shear modulus $\bar{G}\left(\boldsymbol{x}, \theta\right)$ is chosen to lie within the upper range of typical correlation lengths of CPT data [12]. Thus, two correlation lengths are examined: $l_\mathrm{c} = 1$ m and $l_\mathrm{c} = 1.50$ m. The generation of the stochastic shear modulus realizations is performed for a relative truncation error $\epsilon_\mathrm{max} = 0.05$. Figure 6 shows two

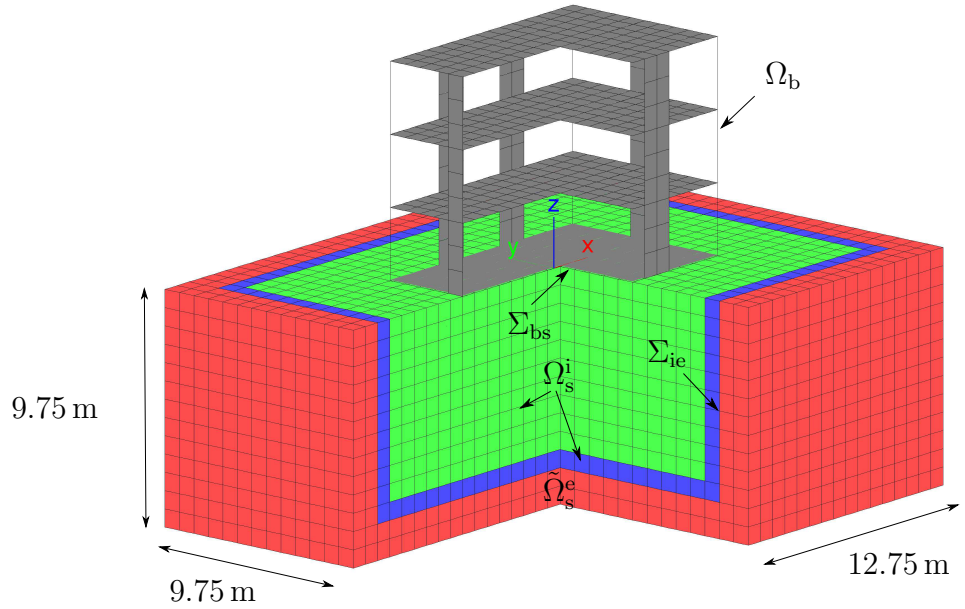

Figure 5: FE-PML model. The shear modulus in the green part of Ω_s^i is modeled as a conditional random field whereas in the blue part it is deterministic. The subdomain definitions are in accordance with figure 1.

realizations of the stochastic shear modulus of the soil mapped onto the finite element mesh for the two correlation lengths considered.

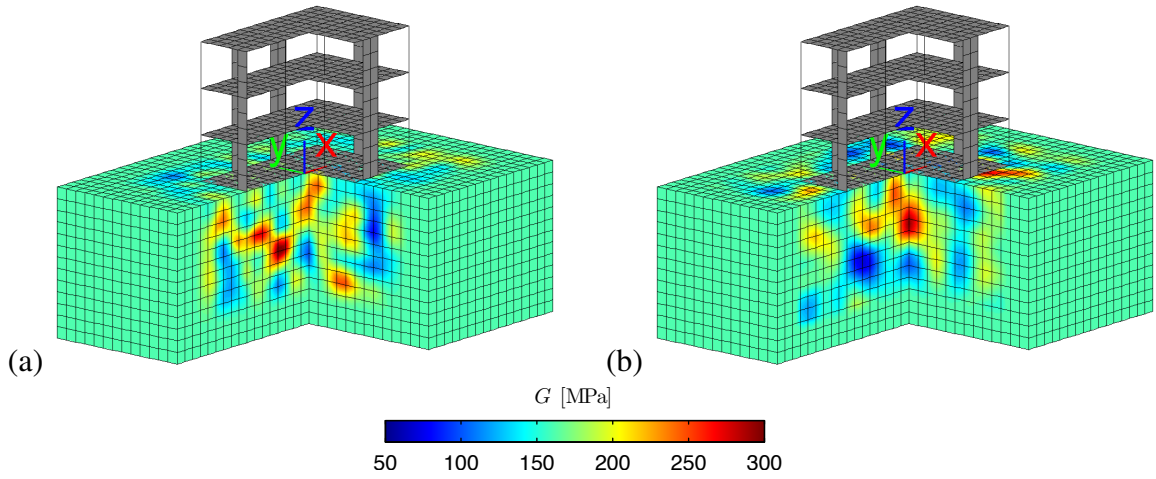

Figure 6: Realizations of the stochastic shear modulus of the soil mapped onto the finite element mesh. Shear modulus with correlation length (a) $l_c = 1$ m and (b) $l_c = 1.50$ m.

In order to understand how the uncertain local subsoil conditions affect the response of buildings to ground-borne vibration, two loading cases are considered, an actual and an artificial. The actual loading case (LC1) is the solution of the problem where the incident wave field propagates through Ω_s^i before it impinges the foundation of the building. This loading case allows to assess the overall influence of the uncertain local subsoil conditions on the response of the building. In this case, the nodal forces $\hat{\underline{f}}_s$ of equation (4) are used to propagate the incident wave field through the FE-PML model. In the artificial loading case (LC2), the incident wave field is applied as nodal forces $\hat{\hat{\underline{f}}}_{\Sigma_{bs}}$ directly on the soil-foundation interface Σ_{bs} according to equation

(5) and assuming it has propagated through the subsoil with the deterministic properties of table 2. The main difference between the two loading cases is that the incident wave field which finally impinges the foundation of the building in LC1 is perturbed by the (stochastic) heterogeneity of $\Omega_{\mathrm{s}}^{\mathrm{i}}$ (figure 7b) whereas in LC2 it is not. The artificial loading case is considered as it provides additional insight by allowing to examine solely how the uncertain subsoil conditions affect the dynamic stiffness matrix of the coupled soil-building system and, equivalently, its modal characteristics.

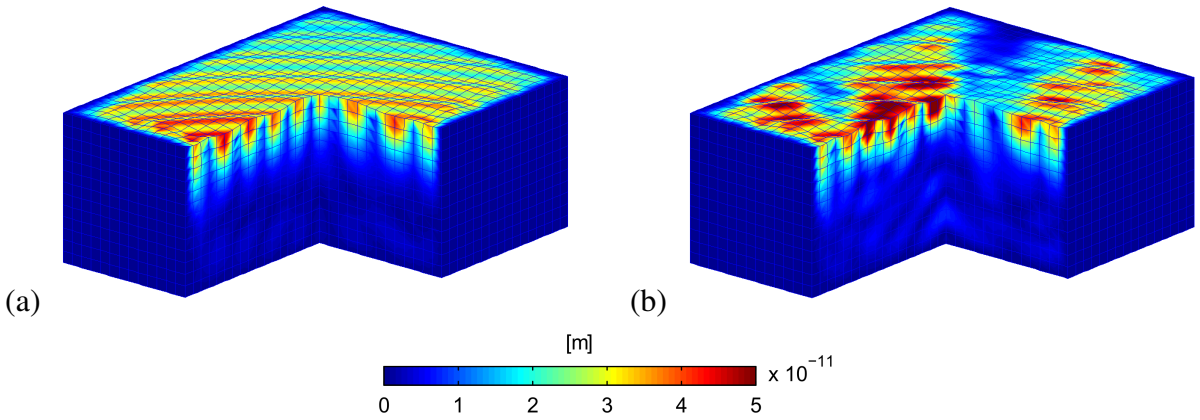

Figure 7: Snapshot of the free field response $\underline{\mathbf{u}}(t) = \mathrm{Re}\left(|\hat{\underline{\mathbf{u}}}|\exp\left(i\omega t + i\angle\hat{\underline{\mathbf{u}}}\right)\right)$ at 80 Hz and $t = 0$. (a) Homogeneous subsoil with the mean properties of table (2) and (b) subsoil with the shear modulus realization of figure 6b.

The uncertainty is propagated from the subsoil properties to the response of the building by means of Monte-Carlo simulation. In total, $n_{\mathrm{R}} = 1000$ realizations are used to estimate the uncertainty on the building response. This uncertainty is quantified by computing the coefficient of variation and by constructing confidence regions for the building response. The former is defined as:

$$\mathrm{CoV}_{|\hat{\underline{u}}_j|} = \frac{\sigma_{|\hat{\underline{u}}_j|}}{\mu_{|\hat{\underline{u}}_j|}} \tag{19}$$

where $\sigma_{|\hat{\underline{u}}_j|}$ and $\mu_{|\hat{\underline{u}}_j|}$ are the standard deviation and the mean value of the response $|\hat{\underline{u}}_j|$ of the j-th degree of freedom. Alternatively, a confidence region with a confidence level of $p_c = 90\%$ for the response $|\hat{\underline{u}}_j|$ can be defined such that:

$$P(|\bar{\underline{u}}_j^l| \leq |\hat{\underline{u}}_j| \hat{\leq} |\hat{\underline{u}}_j^u|) \geq p_c \tag{20}$$

where the lower $|\hat{\underline{u}}_j^l|$ and the upper $|\hat{\underline{u}}_j^u|$ bounds are obtained as the 5% and 95% percentiles of $|\hat{\underline{u}}_j|$ respectively. By utilizing the bootstrap method [18], confidence regions can be also estimated for $\mathrm{CoV}_{|\hat{\underline{u}}_j|}$.

3.1 Free field and foundation response transfer functions

Figure 8 shows the transfer function of receiver F_0 (figure 4) in the z direction for the case where the correlation length of the random field representing the shear modulus of the subsoil is $l_{\mathrm{c}} = 1$ m. The response is presented for the free field without the presence of the building and the cases of the building with raft foundation and the building with individual foundation footings.

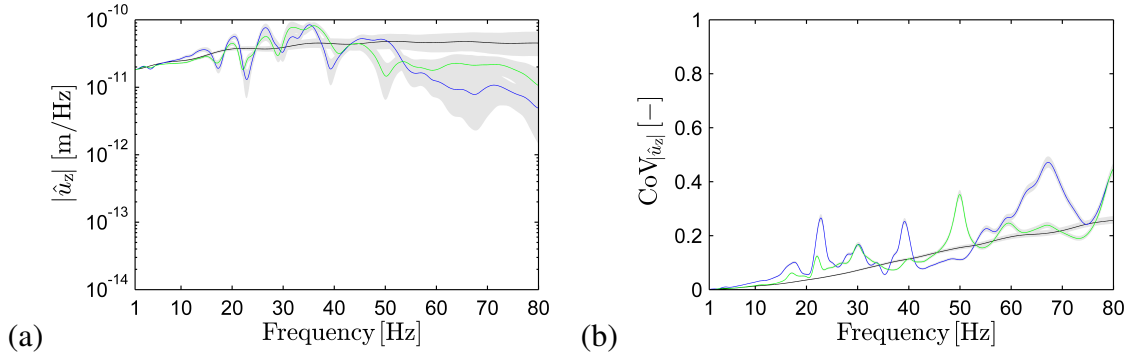

Figure 8: (a) Mean and (b) coefficient of variation of the transfer function of receiver F_0 (figure 4) in the z direction for $l_c = 1$ m. Free field response (black), building with raft foundation (blue) and building with individual foundation footings (green). The 90% confidence regions are shaded grey.

The uncertainty of the free field response of F_0 increases almost linearly with the frequency. After the construction of the building the response of F_0 generally follows a similar trend but with some major difference as the stiffness of the building and especially the foundation affect the response of F_0 in two ways. First, the response near the resonance and antiresonance frequencies of the coupled building-soil system gets amplified and decreased respectively when compared to the free field response [19]. Second, the response at higher frequencies is lower than the free field response for increasing stiffness of the foundation.

3.2 Building response transfer functions

Figures 9 and 10 show the response of receiver A_1 (figure 4) of the building with raft foundation for the two considered correlation lengths l_c of the random field representing the shear modulus of the subsoil. The uncertainty of the response is larger in LC1 than in LC2 as the former includes both the influence of the stochastically perturbed incident wave field and the impact of the stochastic subsoil on the modal characteristics of the coupled soil-building system. In LC1 the uncertainty increases almost linearly with respect to the frequency for the vertical response (figure 9d) while for the horizontal response there are certain frequency bands where the response of the coupled soil-structure system is found to be more sensitive to the subsoil properties (figures 9b and 9b). These frequency bands can be associated with the eigenmodes of the coupled soil-building system that get particularly activated by the induced excitation. As for each realization of the shear modulus of the subsoil the modal characteristics of the coupled system are slightly different and since the response close to resonance frequencies is extremely sensitive to the damping present in the system, frequency bands of increased uncertainty emerge. Similarly, there are other frequency bands in which the structural response is less sensitive. These frequency bands can be associated with eigenmodes of the system that are not sensitive to the subsoil properties. Furthermore, the uncertainty bounds of the response decrease when the stochastic shear modulus of the subsoil has a shorter correlation length. In this case, the wavelength of the elastodynamic waves in the soil is much larger compared to the length scale of spatial fluctuations of the material properties and consequently any local scale variation of the subsoil properties is not resolved in the response.

Figure 11 compares the response of receiver A_1 between the building with raft foundation and the building with individual footings. The correlation length of the random field representing the shear modulus of the subsoil is $l_c = 1$ m. The general trends of the response are in

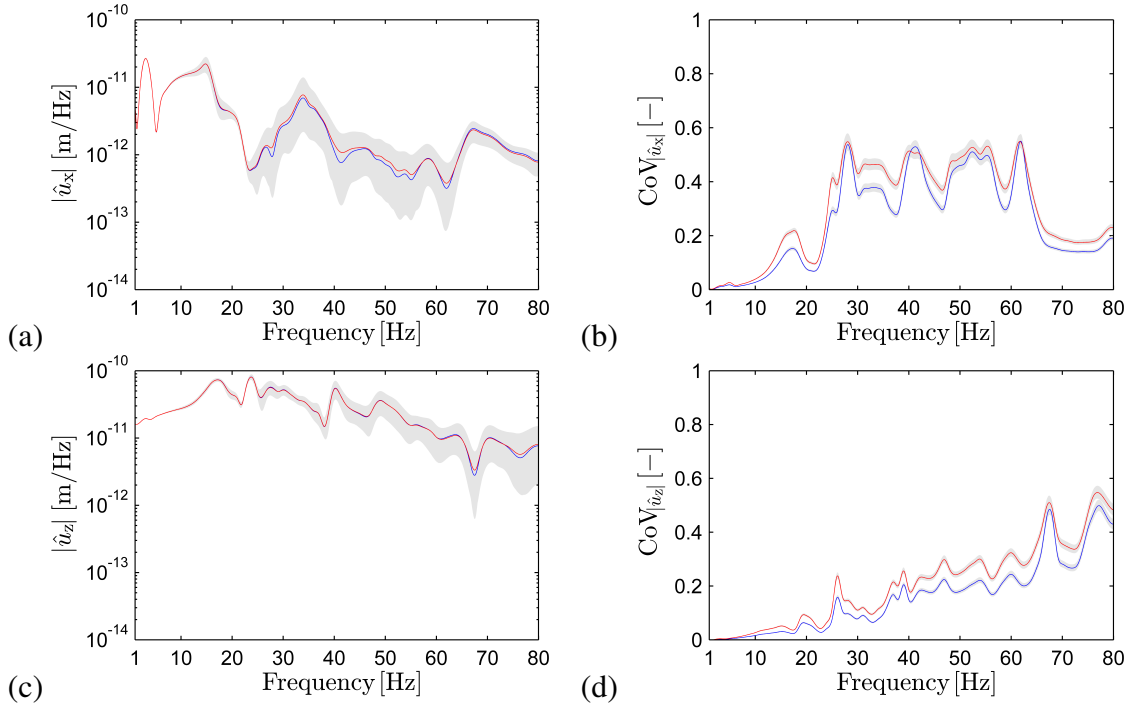

Figure 9: Transfer functions of receiver R_1 (figure 4) for the building with raft foundation and the LC1 with $l_c = 1$ m (blue line) and $l_c = 1.5$ m (red line). (a) Mean and (b) coefficient of variation of the response in the x direction, (c) mean and (d) coefficient of variation of the response in the z direction. The 90% confidence regions are shaded grey.

accordance with the previously stated observations. Nevertheless, the building with individual footings is more sensitive to the subsoil properties, exhibiting higher uncertainty to its response. Because the size of the individual footings is small compared to the scale of variation of the subsoil material properties, each footing rests on top of a soil with different material properties. As a result, the spatial variation of the material properties of the soil cannot be averaged out in the response of the building.

4 CONCLUSIONS

In this paper the influence of the imperfectly known local subsoil conditions on the response predictions of buildings to environmental ground vibration is examined. A parametric analysis is performed with respect to the statistical characterization of the shear modulus of the soil and the foundation type of the building.

The uncertainty of the response of the building is traced on the stochastically perturbed incident wave field that excites the building and the impact of the stochastic subsoil on the modal characteristics of the coupled soil-building system. The correlation length of the stochastic subsoil properties affects the uncertainty bounds of the response of the building. Furthermore, it is demonstrated that the foundation type of the building is a crucial factor determining its response and the associated uncertainty bounds. Generally, the structural response uncertainty increases at higher frequencies. The sensitivity of the structural response to the subsoil properties varies considerably over frequency bands, however.

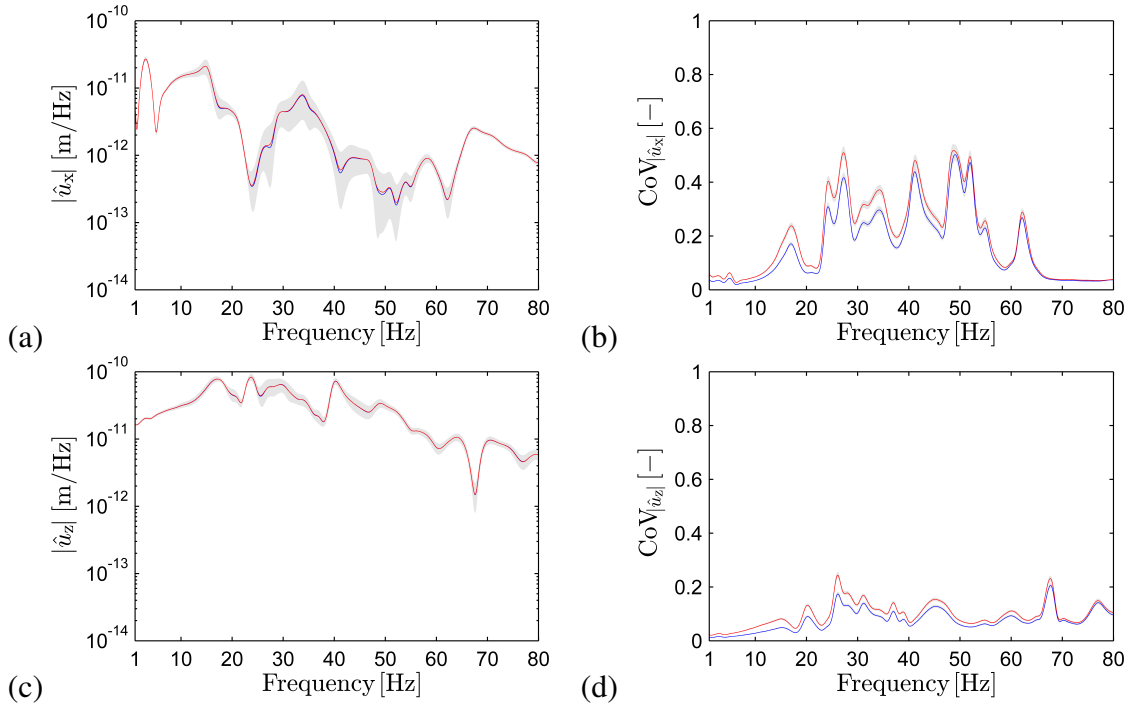

Figure 10: Transfer functions of receiver R_1 (figure 4) for the building with raft foundation and the LC2 with $l_c = 1$ m (blue line) and $l_c = 1.5$ m (red line). (a) Mean and (b) coefficient of variation of the response in the x direction, and (c) mean and (d) coefficient of variation of the response in the z direction. The 90% confidence regions are shaded grey.

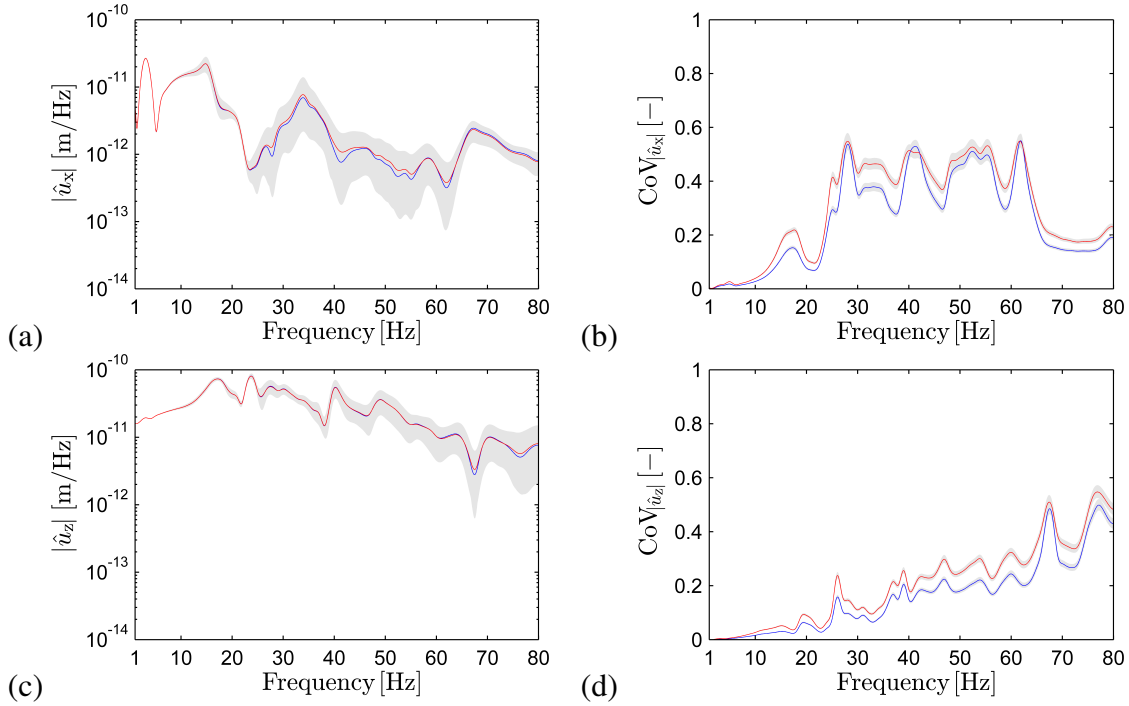

Figure 11: Transfer functions of receiver R_1 (figure 4) for the building with raft foundation (blue line) and the building with individual foundation footings (red line) for the LC1 with $l_c = 1$ m. (a) Mean and (b) coefficient of variation of the response in the x direction, and (c) mean and (d) coefficient of variation of the response in the z direction. The 90% confidence regions are shaded grey.

ACKNOWLEDGMENTS

The research presented in this paper has been performed within the frame of the project OT/13/59 "Quantifying and reducing uncertainty in structural dynamics" funded by the Research Council of KU Leuven. The financial support is gratefully acknowledged.

REFERENCES

[1] J.P. Wolf, *Dynamic soil-structure interaction*, Prentice-Hall, 1985.

[2] D. Clouteau, Degrande G., Lombaert G., Numerical modeling off traffic induced vibrations, *Meccanica*,**36**(4), 401-420, 2001.

[3] G.B. Baecher, J.T.Christian, *Reliability and Statistics in Geotechnical Engineering*, Wiley & Sons, 2003.

[4] E. Savin, D. Clouteau, Elastic wave propagation in a 3D unbounded random heterogeneous medium coupled with a bounded medium. Application to seismic soil-structure interaction (SSSI), *International Journal for Numerical Methods in Engineering*,**54**, 607-630, 2002.

[5] O. Vonestorff, E. Kausel. Coupling of boundary and finite-elements for soil-structure interaction problems. *Earthquake Engineering and Structural Dynamics*, **18**(7), 1065–1075, 1989.

[6] J. Lysmer, R. Kuhlemeyer. Finite dynamic model for infinite media. *Journal of the Engineering Mechanics Division*, **95**(EM4), 859–877, 1969.

[7] F. Medina, J. Penzien. Infinite elements for elastodynamics. *Earthquake Engineering and Structural Dynamics*, **10**(5), 699–709, 1982.

[8] U. Basu, A.K. Chopra, Perfectly matched layers for time-harmonic elastodynamics of unbounded domains: theory and finite-element implementation, *Computer Methods in Applied Mechanics and Engineering*,**192**(11-12), 1337-1375, 2003.

[9] D. Aubry, D. Clouteau, A subdomain approach to dynamic soil-structure interaction, *Recent advances in earthquake engineering and structural dynamics*, V. Davidovici, R.W. Clough eds., Ouest Editions/AFPS, Nantes 251-272, 1992.

[10] P. Coulier, S. François, G. Degrande, G. Lombaert. The influence of source-receiver interaction on the numerical prediction of traffic induced vibrations. *Journal of Sound and Vibration*, **333**(12), 81–86, 2014.

[11] M. Schevenels, S. François, G. Degrande, EDT: An ElastoDynamics Toolbox for MATLAB, *Computers & Geosciences*,**35**(8), 1752-1754, 2009.

[12] M. Huber, Soil variability and its consequences in geotechnical engineering, PhD thesis, Institut für Geotechnik der Universität Stuttgart, 2013.

[13] E. Vanmarcke, *Random Fields: Analysis and Synthesis*, MIT Press Classics, 1983.

[14] P. Liu, A. Der Kiureghian, Multivariate distribution models with prescribed marginals and covariances, *Probabilistic Engineering Mechanics*,**1**(2), 105-112, 1986.

[15] C. Li, A. Der Kiureghian, Optimal discretization of random fields, *Journal of Engineering Mechanics*,**119**(6), 1136-1154, 1993.

[16] A.M. Olsson, G.E. Sandberg, Latin hypercube sampling for stochastic finite element analysis, *Journal of Engineering Mechanics*,**128**(1), 121-125, 2002.

[17] M.H. Santare, Thamburaj P., G.A. Gazonas, The use of graded finite elements in the study of elastic wave propagation in continuously nonhomogeneous materials, *International Journal of Solids and Structures*,**40**, 5621-5634, 2003.

[18] B. Efron, R.J. Tibshirani, *An Introduction to the Bootstrap*, Chapman & Hall, 1993.

[19] S. François, L. Pyl, H.R. Masoumi, G. Degrande. The influence of dynamic soil-structure interaction on traffic induced vibrations in buildings. *Soil Dynamics and Earthquake Engineering*, **27**, 655–674, 2007.